Efficient Multiwavelength Dynamic Model for Erbium-Doped Fiber Amplifier

Alfred W. T. Wu and Arthur J. Lowery, *Senior Member, IEEE*

***Abstract*— An efficient full spectrum (1480–1600 nm) large-signal transient dynamic model of an erbium-doped fiber amplifier (EDFA) is developed. A technique to speed up the simulation by a factor of 1000 using artificial delay lines based on the transmission-line model (TLM) is presented. Simulations and experimental results show the delay line method is not detrimental to the accuracy of the model. The efficiency of this model means it is ideal for simulating the dynamics of large wavelength-division multiplexed (WDM) networks if included in a network simulator.**

***Index Terms*—Erbium-doped fiber amplifiers, modeling.**

I. Introduction

THE ERBIUM-DOPED fiber amplifier (EDFA) has become one of the key components in WDM networks. Its main advantages include high gain, wide bandwidth, and polarization insensitivity [1]. Due to their long excited-state lifetime, EDFA's are immune to channel gain modulation if the lowest modulation component is greater than 10 kHz [2]. This means that channel cross-talk is minimal in high-speed WDM networks during normal network operation. However, channel failures due to accidental component failures or channel switching can produce large-power transients which cause gain transients in the entire WDM network, affecting all channels [9]. As the size and complexity of WDM networks increases, these transient effects may become significant for system performance and reliability. To analyze the effect and behavior of these dynamics in networks using a large number of EDFA's, an efficient numerical model is necessary.

The single-channel large-signal transient behavior of an EDFA was simulated and reported by Ko [3] using a model based on the references in [2] and [4]. However, only the case of a single channel and a single amplified spontaneous emission (ASE) component at a signal wavelength with a bandwidth ($\Delta\lambda$) was considered. However, to fully account for the EDFA dynamics including cross saturation between multiple signals and ASE saturation, it is necessary to include the full EDFA spectrum (1480 to 1600 nm) in a model. This is particularly important when the EDFA is part of a ring-like network which the ASE and the signal would lase (if the round-trip gain exceeds unity) [13], [14] and channels compete with each other for gain. As a result, the EDFA behavior will heavily depend on not just the signal but also the entire ASE spectrum. To predict such behavior can be computationally intensive. To fully account the effects of forward and backward ASE saturation, these simulation models require long execution times which is undesirable when simulating large networks.

In this paper, we have implemented a numerical model of a 1480-nm forward-pumped EDFA. The numerical model fully describes the dynamic response of the EDFA and takes into account the full EDFA spectrum (1460–1600 nm), and the effects of forward and backward ASE saturation. The model requires only simple parameters to be obtained: gain and loss coefficient spectra, intrinsic saturation power, and excited-ion lifetime [5]. We have used a transmission line model (TLM) [6] with extra delay sections to improve the computational efficiency by a factor of 1000. The results of this delay-line method are in excellent agreement with our experimental results.

II. Theory

For a forward two-level pumped EDFA, the carrier density rate equation and the signal power equations along the erbium-doped fiber (EDF) are derived from [7]

$$\frac{dN(x,t)}{dt} = -\frac{N(x,t)}{\tau} - \sum_{\lambda} \frac{P_{\lambda}^{f}(x,t) + P_{\lambda}^{b}(x,t)}{P_{\lambda}^{\mathrm{sat}}\tau} \times \left[N(x,t) - \frac{\alpha_{\lambda}}{\alpha_{\lambda} + g_{\lambda}} \right] \tag{1a}$$

$$\frac{dP_{\lambda}^{f}(x,t)}{dx} = N(x,t)\left[(\alpha_{\lambda} + g_{\lambda})P_{\lambda}^{f}(x,t) + 2h\nu\Delta\nu g_{\lambda}\right] - \alpha_{\lambda}P_{\lambda}^{f}(x,t) \tag{1b}$$

$$\frac{dP_{\lambda}^{b}(x,t)}{dx} = N(x,t)\left[(\alpha_{\lambda} + g_{\lambda})P_{\lambda}^{b}(x,t) + 2h\nu\Delta\nu g_{\lambda}\right] - \alpha_{\lambda}P_{\lambda}^{b}(x,t) \tag{1c}$$

where g, α are the gain and loss coefficients per unit length [5], P_{sat} is the intrinsic saturation power [7], τ is the exited-state lifetime, N is the normalized excited-state ion population, ν is the signal frequency with mean bandwidth $\Delta\nu$, h is Planck's constant, and P^{f} and P^{b} are the forward and backward traveling signal powers, respectively.

The assumptions in (1) are:

- the EDF gain spectra is homogeneously broadened;
- all signal mode fields along the fiber are approximated by Gaussian mode distributions and the overlap factor

Manuscript received November 3, 1997; revised May 6, 1998.

The authors are with Australian Photonics Cooperative Research Centre, Photonics Research Laboratory, Department of Electrical and Electronics Engineering, The University of Melbourne, Parkville, Vic. 3052, Australia.

Publisher Item Identifier S 0018-9197(98)05398-6.

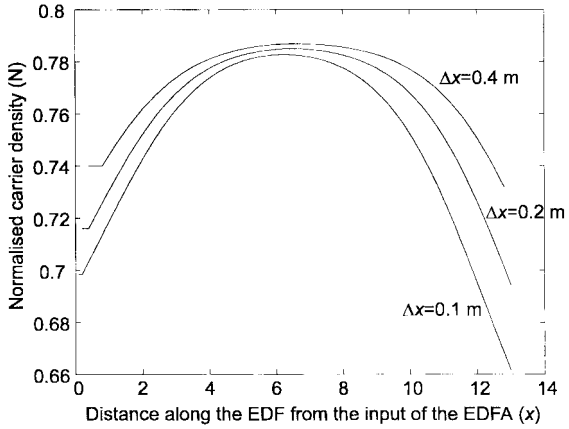

Fig. 1. Normalized excited-ion distribution along EDF at $\Delta x = 0.1$, 0.2, and 0.4 m in the steady state with 200-mA pump current.

between the mode and the doped area is independent of the respective signal power, i.e., the doping area is confined near to the center of the core [7];

- the signal gain is polarization-independent;
- the dopant concentration is small enough that pair-induced quenching (PIQ), which dominates over the homogeneous cooperative process, background loss and excited states absorption, can be ignored [8].

The gain coefficient $g(\lambda)$ can be determined by a simple experiment such as passing a high pump power through a very short length of fiber (<0.3-dB length of loss) [5]. The loss coefficient, $\alpha(\lambda)$, spectrum can be obtained by a simple cut-back experiment. Once the intrinsic saturation power of a particular wavelength is obtained from a transmission measurement, the intrinsic saturating power (P^{sat}) of the complete spectrum can be easily determined using the gain and loss coefficients. The time constant (τ) is obtained by measuring the ASE output decay of an EDF being excited by pump pulses [9]. As a result, only parameters $g(\lambda)$, $\alpha(\lambda)$, P_λ^{sat} (at any particular wavelength λ), and τ are required to fully characterized the EDFA's dynamics.

It can be seen from (1a) that the excited ion population is power-dependent. Since the signal powers vary along the EDF [from (1b) and (1c)], the gain varies along the fiber as well. To investigate the effects of using finite sections in the model, (1a)–(1c) were solved for the steady-state (setting (1a) to zero) by using a two-boundary finite-element relaxation method [10]. The results are shown in Fig. 1. It can be seen that the normalized excited-ion population varies along the EDFA nonlinearly, with the gain at the ends of the EDF heavily saturated by ASE. As a result, different section size results in different accuracy. Therefore, to maintain accuracy, it is necessary to divide the EDF into short sections.

The ASE components in (1b) and (1c) depend on the width of the wavelength interval, $\Delta\lambda$, that the EDFA spectrum is divided into. Since the forward and backward ASE saturates the gain along the EDFA, due to the discretization of the gain coefficient, loss coefficient and intrinsic saturation power spectra, the choice of $\Delta\lambda$ also affects the excited-ion population along the EDFA and hence the steady-state accuracy. In the case of EDFA dynamics in a ring-like structure, where lasing

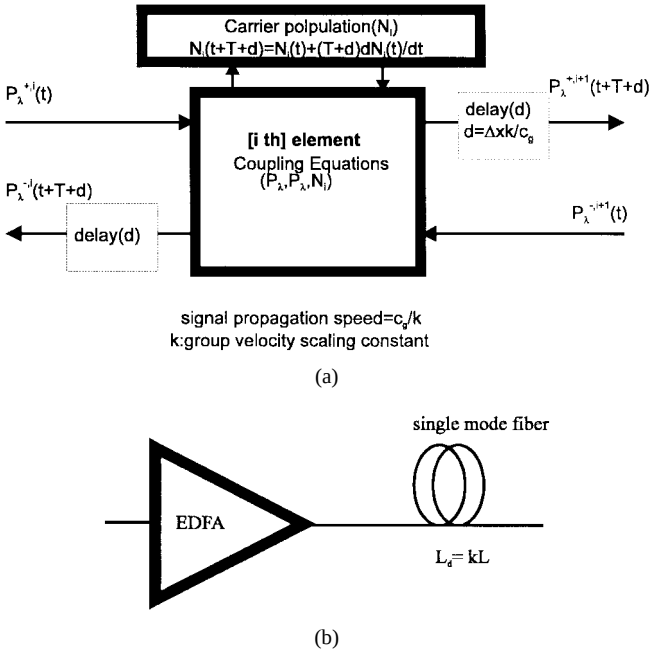

Fig. 2. (a) Numerical model of a section of an EDFA. (b) An equivalent EDFA model used for simulations when the delay line method is used.

of ASE components is possible, the choice of $\Delta\lambda$ becomes even more important.

III. Numerical Model

To solve (1), the EDF is divided into sections of equal length (Δx). The carrier density is assumed to be constant within a section, as illustrated in Fig. 2. The whole EDFA spectrum (including the pump spectrum), from 1460 to 1600 nm, is divided into discrete signal wavelengths with a mean width $\Delta\lambda$ $(\lambda\Delta\nu/\nu)$. The discrete algorithms, derived from (1), for the computation are shown as follows:

$$N^i(t+\Delta T) = N^i(t) + \frac{dN^i(t)}{dt}\Delta T \tag{2a}$$

$$\frac{dN^i(t)}{dt} = -\frac{N^i(t)}{\tau} - \sum_\lambda \frac{P_\lambda^{f,i}(t) + P_\lambda^{b,i}(t)}{P_\lambda^{\text{sat}}\tau} \times \left[N^i(t) - \frac{\alpha_\lambda}{\alpha_\lambda + g_\lambda}\right] \tag{2b}$$

$$P_\lambda^{f,i+1} = P_\lambda^{f,i} + \left(N^i(t)\left[(\alpha_\lambda + g_\lambda)P_\lambda^{f,i} + 2h\nu\Delta\nu g_\lambda\right] - \alpha_\lambda P_\lambda^{f,i}(t)\right)\Delta x \tag{2c}$$

$$P_\lambda^{b,i} = P_\lambda^{b,i+1} + \left(N^i(t)\left[(\alpha_\lambda + g_\lambda)P_\lambda^{b,i+1} + 2h\nu\Delta\nu g_\lambda\right] - \alpha_\lambda P_\lambda^{b,i+1}(t)\right)\Delta x. \tag{2d}$$

The transient simulations are initialized from the steady-state solution obtained by setting (2b) to be zero. Since the steady-state solution is relatively simple, it will not be discussed in great detail here. As it was shown earlier, the choice of Δx and $\Delta\lambda$ affect the accuracy of the steady-state excited-ion distribution and thus the initial gain and ASE along the fiber. As a result, the dynamic solution is also likely to be affected. Depending on the magnitudes of g and α (which depend on the individual EDFA), optimal values of Δx, Δt and $\Delta\lambda$ are

necessary in order to balance the simulation accuracy and execution time.

At each new iteration with, time increased by a time step (Δt), a new carrier density (N^i), forward propagating signal $(P_\lambda^{f,i})$, forward ASE $(P_\lambda^{f,i})$, and backward ASE $(P_\lambda^{b,i})$ are computed for each section. If we use the TLM, the section length (Δx) and the time step (Δt) are related by $\Delta x = \Delta T c_g$, where c_g is the signal group velocity. If the decay time of the large-signal transient is $\tau_{\rm dyn}$, then the minimum required number of iterations (n) is

$$n = (\tau_{\rm dyn} c_g)/\Delta x.$$

That means, for $\Delta x = 0.1$ m, $c_g = 2\times10^8$ ms^{-1} (assuming a group refractive index of 1.5 in silica fiber) and a 10-ms transient simulation, the required number of iterations (n) per signal is at least 2×10^7. The execution time of the simulation depends on the number of iterations multiplied by the number of sections and the number of wavelengths (1480 to 1600 nm). In order to fully describe the full-bandwidth dynamics of saturated EDFA's of an WDM network in a reasonable time, it is necessary to reduce the "effective time-step" carried out in a simulation to improve the simulation efficiency while maintaining accuracy.

To improve the simulation efficiency, we introduce a delay factor, k. This is equivalent to introducing an additional propagation delay within each fiber section (Fig. 2). This can be thought of as introducing lossless lengths of fiber between gain sections. As a result of this, the number of iterations is reduced to

$$n = \tau_{\rm dyn} c_g/(k\Delta x).$$

Increasing the EDFA's length by a factor of k affects the rate (or dynamics) that forward and backward signal saturate the different sections of EDFA. However, if the delay is not significant compared to the excited-state lifetime ($\sim$ms) and the rate of change of the input signal power ($\sim\mu$s), then the effect on the dynamics of the EDFA will be insignificant. Our results in the next section show that delay scaling reduces execution time dramatically while maintaining the accuracy of the EDFA dynamics.

Delay scaling results in a fixed delay of the entire output response with respect to a change in the input power, simply because the delay of the fiber has been increased k times. Therefore, the delay-scaled transient model is similar to an EDFA with its output connected to a lossless and nondispersive single-mode fiber (SMF) of length L_d where $L_d = L(k-1)$ and L is the actual length of the EDFA [Fig. 2(b)]. For example, for a 13-m EDF, a simulation using a k of 1000 requires an L_d of 13 km. In this case, the computation time is reduced by approximately 1000 times (see Section IV). Furthermore, as EDFA's are used as signal repeaters (or power boosters) in networks, distances between EDFA's are in the order of kilometers. As a result, the additional delay can be accommodated in actual networks.

For all of the simulations discussed in this paper, Δx and $\Delta\lambda$ are chosen to be 0.1 m and 1 nm, respectively. The EDFA spectrum is modeled from 1460 to 1600 nm.

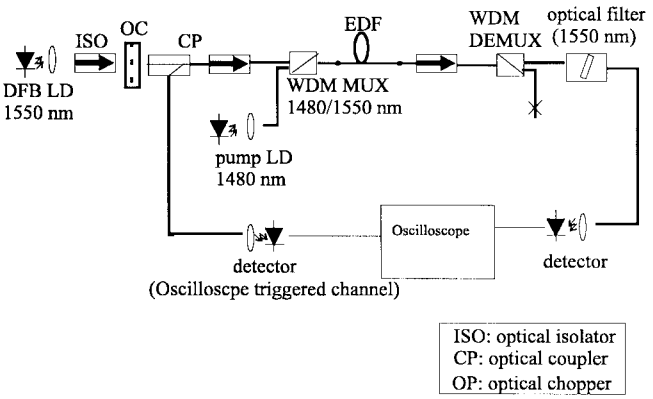

Fig. 3. Experiment for large-signal single channel dynamics.

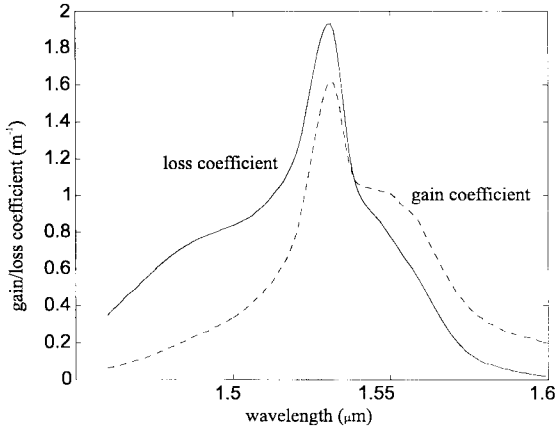

Fig. 4. Gain and absorption spectra.

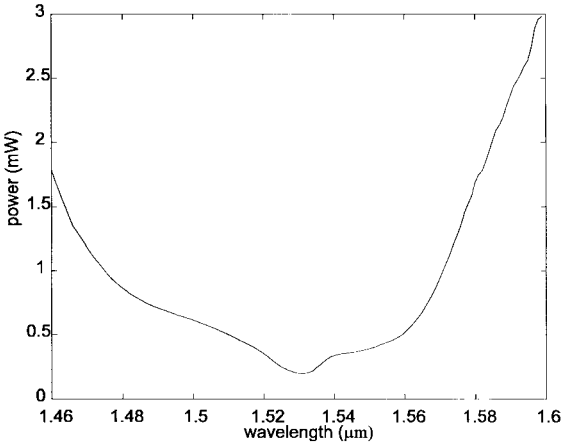

Fig. 5. Intrinsic saturation power spectrum.

IV. Experimental and Simulation Results

A. Single-Channel Large-Signal Dynamics

Fig. 3 shows the experimental setup for demonstrating the large-signal saturation dynamics of a single channel. The results of this experiment were compared with simulations with $k = 1$ and $k = 1000$. In this experiment, the EDFA has a 13-m-long aluminum codoped erbium fiber with a 1480-nm pump laser arranged in a forward pumping scheme. The

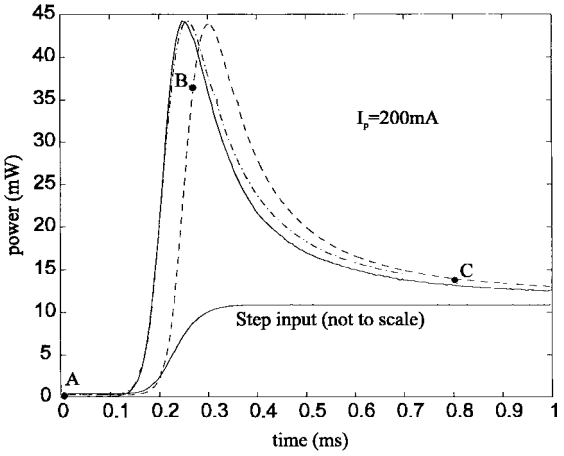

(a)

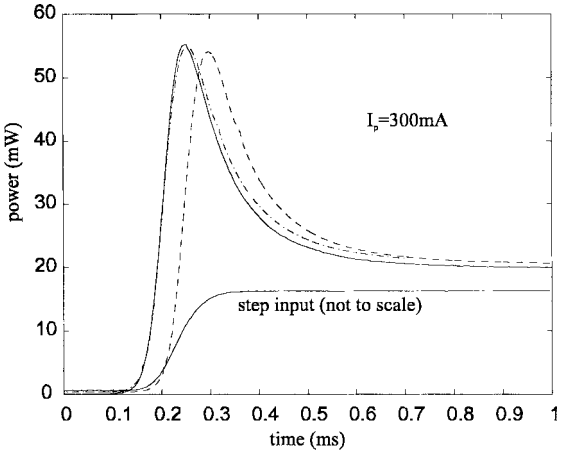

(b)

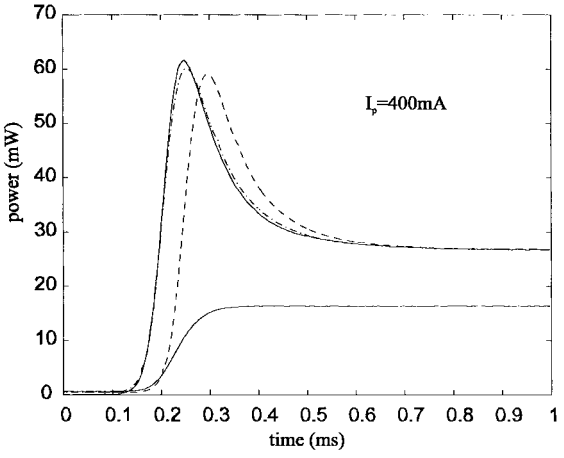

(a)

Fig. 6. Large-signal response at I_p = (a) 200 mA, (b) 300 mA, and (c) 400 mA. Solid line: experimental measurement. Dashed line: simulation result with $k = 1000$. Dashed and dotted line: simulation results with $k = 1$.

gain coefficient, loss coefficient, and intrinsic saturating power spectra are shown in Figs. 4 and 5. The carrier lifetime was measured to be ~9.2 ms by using techniques mentioned earlier. A 1550-nm DFB laser operating under CW conditions was passed through an optical chopper to produce a 200-Hz step-like optical input (~ 0.1-ms rise-time) to the EDFA. The

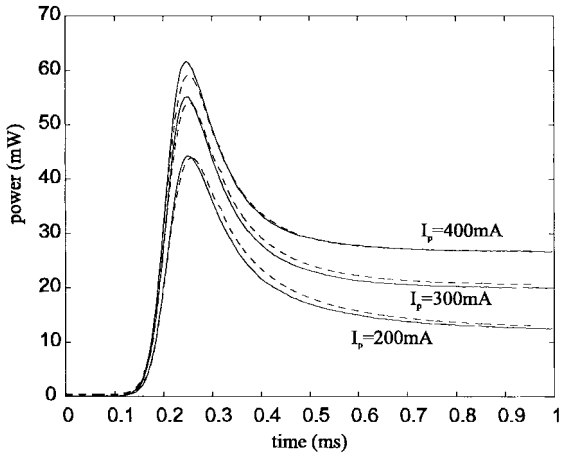

Fig. 7. Large-signal response to a step input. Solid line: experimental measurement. Dashed line: simulation result time advanced by 43 μs due to delay introduced by $k = 1000$.

TABLE I
COMPARISON OF CPU TIME VERSUS DELAY FACTOR (k) USING A 50-MHZ SPARC CPU

Delay factor k	CPU time required for simulation in seconds
1	187224
100	1849
1000	186

shape of these input pulses were modeled and implemented in the simulation. The input signal pulses are also coupled to the photodetector to trigger the oscilloscope. The EDFA output is filtered at 1550 nm and connected to the oscilloscope through a photodetector. The bandwidth of the photodetector is 125 MHz and the oscilloscope has a 200-MHz bandwidth.

The results of this experiment were compared with the simulation results with $k = 1$ and $k = 1000$. The output coupling loss between the EDFA and the photodetector was estimated to be 5.4 dB by comparing the output signal's peak between the experimental and simulation results, at a 200-mA pump current. In Fig. 6, there are excellent agreements between the simulation and experimental results for three different pump powers. The small difference at the output power peak is mainly due to the finite value chosen for Δx and $\Delta\lambda$ as explained in the steady-state discussion in the previous section. Fig. 6 also shows the simulation results using $k = 1000$ (i.e., an additional delay of 0.33 μs between sections). In this case, the execution time is reduced by approximately 1000 times and the additional delay (43 μs) of the output can be seen (as mentioned in the previous section). These time-shifted results are in excellent agreement with the experimental results for all three pump power levels as shown in Fig. 7. The use of the delay-line method reduces CPU time required for executing simulations. The CPU time required for various values of k ranging from 1 to 1000 is shown in Table I.

Fig. 8 shows the simulated EDFA optical output spectrum at $I_p = 200$ mA and $k = 1000$. The simulated output spectra A, B, and C were sampled at 0, 0.25, and 0.8 ms, respectively [corresponding to points A, B, and C in Fig. 6(a)]. These

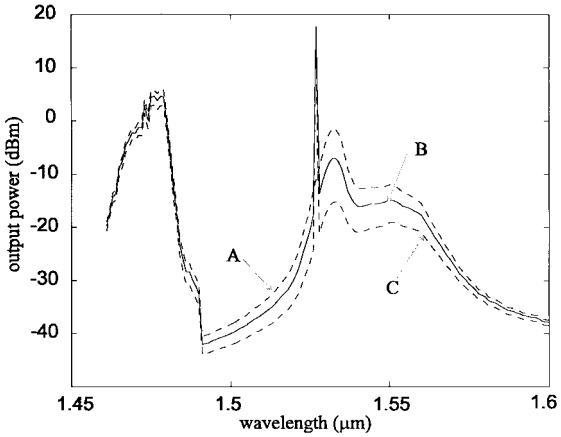

Fig. 8. Simulated EDFA output power spectrum at different time of the simulation for $k = 1000$.

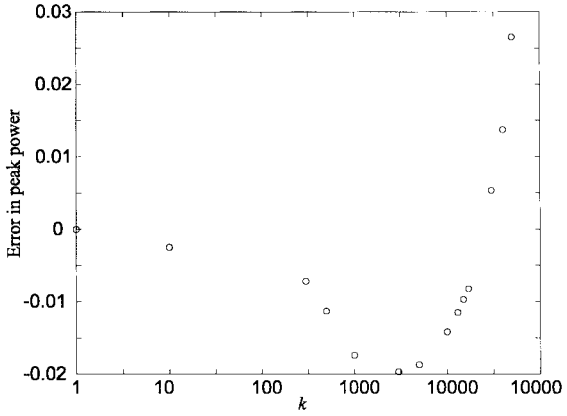

Fig. 9. Change in output peak power level verses k. The y axis represents value of $(P(k) - P_0)/P_0$, where P_0 is the peak output power when $k = 1$ and $P(k)$ is the peak output power for k not equal to 1.

spectra include the pump spectrum from 1460 to 1480 nm which shows the many modes of the pump source. This highlights the effectiveness of the model as it is not limited to a single-wavelength approximation of the pump spectrum. In the experiment, the pump band is removed by the WDM coupler at the output of the EDFA. The dynamics of the gain compression spectrum can also be seen from these spectra, highlighting the ability of our model to also predict multiwavelength dynamics.

B. Effect of Delay Scaling

The overall effect of the delay scaling is to slow down the propagation of signal, and the forward and backward ASE with respect to the change of the input signal and the excited state population decay. The degree of these effects (i.e., the distortion of the actual dynamics of the EDFA) can be assessed by examining the change in output peak power verses k at $I_p =$ 300 mA, as plotted in Fig. 9. As k increases, a longer time is required for the input pulse to travel through the EDF. The delay provides more time for the excited state population to saturate at the input end of the fiber which reduces the gain of the later parts of the pulse. As a result, the gain experienced by the signal is lower than it should be.

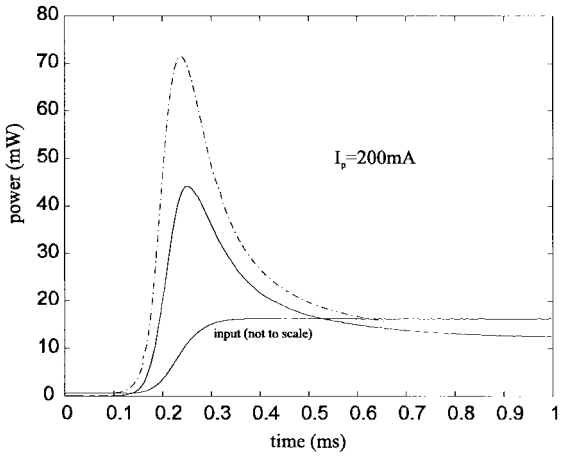

Fig. 10. Simulated large-signal response assuming no ASE (solid line). The experimental result is shown as a dashed line.

However, as k is further increased beyond 3000, the peak power starts to increase. This is due to the quantization error resulted from sampling the rising edge of the input pulses (i.e., the modulated signal at 1550 nm). The sampling time-step increases with increasing k; therefore, if k is large enough, the rising edge of the sampled input resembles a "staircase"-like signal with each step behaving like a large signal with a zero rise time. As a result, for large k ($>$3000), the peak power increases with increasing k. This effect is particularly significant if the rise-time of the input pulses is comparable to the fluorescence lifetime of the EDFA. On the other hand, if the rise time is small (e.g., $\sim$ns), the input pulses behaves as real step inputs and, as a result, the quantization error is insignificant. In real WDM systems, depending on the type of wavelength switching devices, switching times vary from the order of milliseconds to nanoseconds [15]. Therefore, implementing the delay-line technique in dynamic simulations, the rise time (switching time) of the large signal must be considered to obtain the required accuracy and efficiency.

In order to confirm the effect of forward and backward ASE on the EDFA dynamics, and hence the necessity of including these terms, the simulation was run with the zero ASE in (2b) and (2c). In the case of zero ASE, before the arrival of the signal pulse, the upper level population is higher than with ASE. This causes a higher gain along the EDF which results in a higher peak power. This large signal gain causes a high rate of stimulated emission and hence the transient state decays faster to the steady state. At steady state, because the signal level is much higher than the ASE, the discrepancy from the actual signal level is very small, as shown in Fig. 10.

C. ASE Dynamics

To verify the ASE dynamics predicted by the model experimentally, the pump laser was modulated using an optical chopper. Two lengths, 6 and 13 m, of aluminum codoped erbium fiber were used. The responsivity of the photodetector at the EDFA output was assumed to be close to its 1550-nm value over the range 1500 nm to 1600 nm (within $\pm$0.01 mA/mW). These ASE dynamics are shown in Fig. 11. The shorter the length of the EDF, the sooner the response

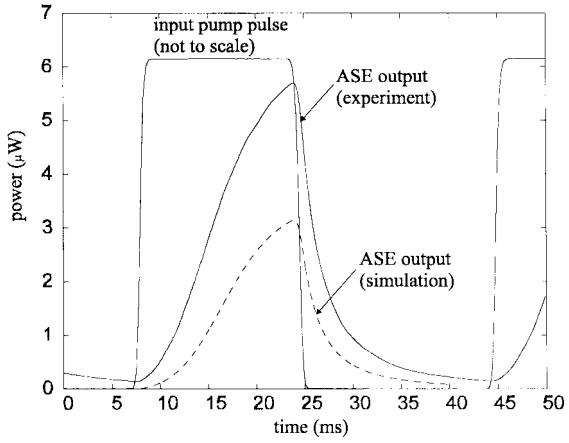

(a)

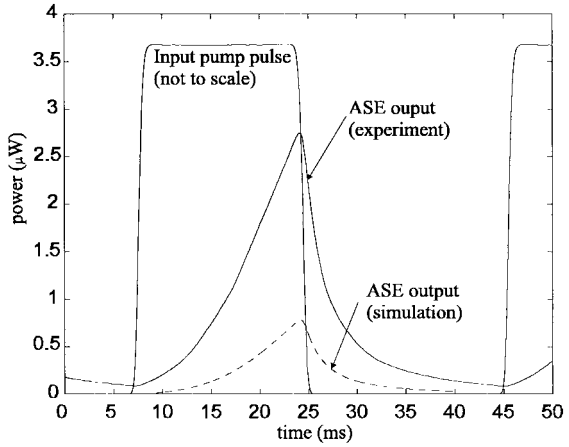

(b)

Fig. 11. ASE dynamics by chopping pump input at $I_p = 400$ mA using (a) a 6-m-long EDF and (b) a 13-m-long EDF.

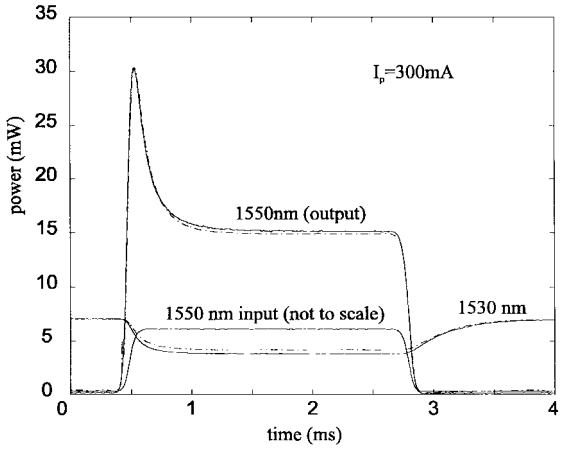

(a)

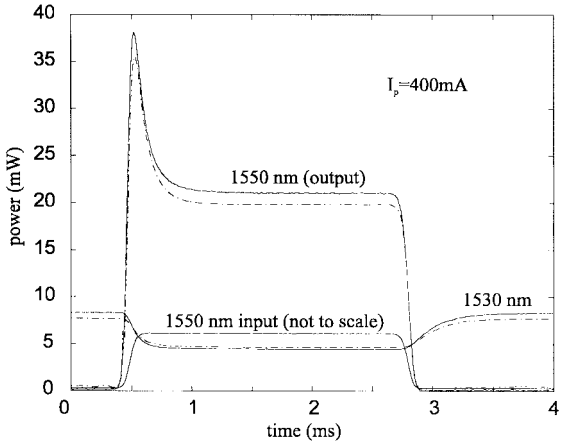

(b)

Fig. 12. WDM signal transient at $I_p =$ (a) 300 mA and (b) 400 mA. Solid line: experimental result. Dashed line: simulation result.

reaches the steady state. This is shown in the experiment and simulation results. Because of the short period of the pump modulation, the ASE signal was not able to decay completely to zero. This means the upper level population is nonzero at the instant of the next rising edge of the pump pulse. This accounts for the extra gain of the experimental results as compared to that of the simulation. Coupling losses also introduced errors in the experiment.

D. Two-Channel Cross-Talk Experiment

Channel switching in WDM networks causes large-signal gain transients in the network. Therefore it is important that the model is able to simulate a similar situation. A two-channel cross-talk experiment was set up which is similar to Fig. 3 except that two CW DFB lasers were used as sources of two WDM channels. The 1550-nm DFB laser was passed through a chopper before coupling into the EDFA. The 1570-nm DFB laser was unmodulated. A simulation was run with $k = 1000$, and the simulation results were time-shifted to account for the additional delay. Fig. 12 shows that the experimental results and the simulations are in excellent agreement at two different pump levels. In the case of $I_p = 400$ mA, the discrepancy of the signal peak is due to the introduction of artificial delays and the discretization of $\Delta\lambda$ and Δa, as explained earlier.

V. Discussion

The model described by (2) assumes the gain medium is homogeneously broadened. To include the effect of inhomogeneous gain broadening, modification of the original model is required with additional parameters such as cross-section spectra and normalized inhomogeneous broadening distribution [11]. Study shows that effects of inhomogeneous medium on gain saturation in alumino-silicate glasses are small and hence both homogeneous and inhomogeneous model provide accurate descriptions of ASE output spectrum [11]. Indeed, modeling the transient behavior of EDFA's based on inhomogeneous gain broadening requires a highly complicated model. The effect of inhomogeneity on the dynamic behavior of EDFA will require further study.

The delay-line method was implemented in the simulation model assuming the doping area is confined near the center of the core. Indeed, the delay-line method is not restricted to be used with such a condition (i.e., radial-independent). Since the delay-line method only increased the effective time step, it can also be implemented in a model where the propagation of mode power is radial-dependent.

In addition to two-level systems, the delay-line method can also be used in three-level systems (e.g., 980–nm pumped EDFA's) provided that the dynamic of the system is preserved, such as the dynamic of the pump excited-state (level 3). In general, $\tau_{3/2}/\tau_{2/1} \sim 10^{-2}$–$10^{-3}$ [2] where $\tau_{3/2}$ and $\tau_{2/1}$ are the nonradiative lifetime of levels 3 and 2, respectively. Therefore, in order to preserve the dynamics of the system, the delay introduced $(c_g/(k\Delta x)$ is required to be less than $\tau_{3/2}$ depending on the required accuracy and improvement on computing efficiency.

Inhomogeneous upconversion due to PIQ is likely to limit the amount of allowable delay introduced when the delay-line method is employed. For alumina co-doped fibers, the timescale for the homogeneous upconversion is in milliseconds and for the inhomogeneous isin submicroseconds [12]. Hence, the delay-line method can be implemented in a model which includes homogeneous upconversion process. The effect and performance of employing the method on such a model is likely to be similar to the model represented by (1) and (2). On the other hand, for dopant concentration within 20×10^{24} m^{-3} and 64×10^{24} m^{-3}, PIQ dominates over homogeneous upconversion (as well as homogeneous cooperative process). As a result, improvement on computing speed and the accuracy of employing the delay-line method are likely to be reduced. The effect of employing delay-line method in PIQ dominated systems require further study.

Furthermore, in this paper, the EDFA spectrum was modeled from 1460 to 1600 nm. As it can be seen in Figs. 4 and 8, due to the low gain coefficient, the ASE outside 1530–1560 nm is likely to cause insignificant saturation to the EDFA. Therefore, by employing the delay-line method, the execution time can be further reduced by considering the main bandwidth of the EDFA (e.g., 1530 to 1560 nm) within the required accuracy.

VI. Conclusion

The simulation model described in this paper accurately describes the multiwavelength dynamic behavior of an EDFA assuming polarization gain-independent homogeneous broadening and negligible pair-induced quenching. The model has been justified by comparison with experiment results. In addition, by introducing additional delays between each section, the execution time can be decreased by a factor of 1000 while keeping within a 2% error. To maintain accuracy, the amount of delay introduced has to be insignificant compared to the excited-state lifetime and the rate of change of the input signal has to be taken into account. In conclusion, the delay-line method enables efficient simulations of large WDM networks employing a large number of EDFA's.

Acknowledgment

The authors would like to thank S. Guy of the Australian Photonics Cooperative Research Centre, Optical Fiber Technology Centre, University of Sydney, NSW, Australia, for providing intrinsic parameters of the erbium doped fiber for reference. The authors also thank G. Smith and Dr. M. Summerfield of Photonics Research Laboratory of the University of Melbourne for fruitful discussions.

References

[1] P. Wysocki and V. Mazurczyk, "Polarization dependant gain in erbium-doped fiber amplifiers: Computer model and approximate formulas," *J. Lightwave Technol.*, vol. 14, pp. 572–584, 1996.
[2] E. Desurvire, "Analysis of transient gain saturation and recovery in erbium doped fiber amplifier," *IEEE Photon. Technol. Lett.*, vol. 1, pp. 196–199, 1989.
[3] K. Y. Ko, M. S. Demokan, and H. Y. Tam, "Transient analysis of erbium doped fiber amplifier," *IEEE Photon. Technol. Lett.*, vol. 6, pp. 1436–1438, 1994.
[4] C. R. Giles, E. Desurvire, and J. R. Simpson, "Transient gain and crosstalk in erbium-doped fiber amplifier," *Opt. Lett.*, vol. 14, pp. 880–882, 1989.
[5] C. R. Giles, C. A. Burrus, D. J. DiGiovanni, N. K. Dutta, and G. Raybon, "Characterization of erbium doped fibers and application to modeling 980 nm and 1480 nm pumped amplifier," *IEEE Photon. Technol. Lett.*, vol. 3, pp. 363–365, 1991.
[6] A. J. Lowery, "New inline wideband dynamic semiconductor laser amplifier model," *Proc. Inst. Elect. Eng.*, vol. 135, pt. J, pp. 242–250, 1988.
[7] C. Giles and E. Desurvire, "Modeling erbium doped fiber amplifiers," *J. Lightwave Technol.*, vol. 9, pp. 271–283, 1991.
[8] P. Mylinski, D. Nguyen, and J. Chrostowski, "Effects of concentration on the performance of erbium doped fiber amplifiers," *J. Lightwave Technol.*, vol. 15, pp. 112–119, 1997.
[9] J. Chung and D. Y. Kim, "Dynamics performance of the all-optical gained-controlled EDFA cascade in multi-wavelength add/drop networks," in *Int. Conf. on Integrated Optics and Optical Fiber Communications and Eur. Conf. on Optical Communication*, 1997, vol. 2, pp. 139–142, paper 448.
[10] E. Dessurvire, *Erbium Doped Fiber Amplifiers*. New York: Wiley, 1994.
[11] E. Desurvire, J. Sulhoff, J. Zyskind, and J. Simpson, "Study of spectral dependence of gain saturation and effect of inhomogeneous broadening in erbium-doped aluminosilicate fiber amplifiers," *IEEE Photon. Technol. Lett.*, vol. 2, pp. 653–655, Sept. 1990.
[12] P. Myslinski, J. Fraser, and J. Chrostowski, "Nanosecond kinetics of upconversion process in EDF and its effect on EDFA performance," in *Proc. Opt. Amplifiers and Their Appl.*, Davos, Switzerland, June 15–17, 1995, vol. ThE3-1, pp. 100–103.
[13] K. Bala and C. Bracket, "Cycles in wavelength routed optical networks," *J. Lightwave Technol.*, vol. 14, pp. 1585–1594, July 1996.
[14] J. Iness, B. Ramamurthy, B. Mukherjee, and K. Bala, "Estimation of all-optical cycles in wavelength routed optical networks," *J. Lightwave Technol.*, vol. 14, pp. 1207–1217, June 1996.
[15] M. Erman, "What technology is required for the Pan-European network, what is available and what is not," in *22nd Eur. Conf. on Optical Communication, ECOC'96 Proc.*, vol. 5, Tub. 2.2.

Alfred W. T. Wu received the B.S. degree in electrical engineering from the University of Alberta, Edmonton, Canada, in 1990. He is currently working toward the Master of Applied Science degree in the Photonics Research Laboratory of the Department of Electrical and Electronics Engineering of the University of Melbourne, Parkville, Vic. Australia.

He was employed by the Spaceborne Control and System Engineering Division of Toshiba Corporation, Japan. After that he was involved in the development of the Global Positioning System receiver in Canada. His research interests include the saturation dynamic of erbium-doped fiber amplifiers and its application in wavelength division multiplexing optical ring network.

Arthur J. Lowery (M'92–SM'96), photograph and biography not available at the time of publication.